Taylor & Francis
Taylor & Francis Group

Philosophical Magazine

ISSN: 1478-6435 (Print) 1478-6443 (Online) Journal homepage: http://www.tandfonline.com/loi/tphm20

Atomic-scale mapping of twins and relevant defective structures in $Al_{20}Cu_2Mn_3$ decagonal approximant

J. Wang, B. Zhang, Z. B. He, B. Wu & X. L. Ma

To cite this article: J. Wang, B. Zhang, Z. B. He, B. Wu & X. L. Ma (2016) Atomic-scale mapping of twins and relevant defective structures in $Al_{20}Cu_2Mn_3$ decagonal approximant, Philosophical Magazine, 96:23, 2457-2467, DOI: 10.1080/14786435.2016.1205229

To link to this article: http://dx.doi.org/10.1080/14786435.2016.1205229

PHILOSOPHICAL MAGAZINE, 2016
VOL. 96, NO. 23, 2457–2467
http://dx.doi.org/10.1080/14786435.2016.1205229

Taylor & Francis
Taylor & Francis Group

Atomic-scale mapping of twins and relevant defective structures in $Al_{20}Cu_2Mn_3$ decagonal approximant

J. Wang[a†], B. Zhang[a†], Z. B. He[b], B. Wu[a] and X. L. Ma[a]

[a]Shenyang National Laboratory for Materials Science, Institute of Metal Research, Chinese Academy of Sciences, Shenyang, China; [b]State Key Laboratory for Advanced Metals and Materials, University of Science and Technology Beijing, Beijing, China

ABSTRACT

Twins or multiple twins occur frequently in the orthorhombic $Al_{20}Cu_2Mn_3$ approximant of decagonal quasi crystal (DQC). Due to the specific structural units, the twins in the $Al_{20}Cu_2Mn_3$ approximant usually exhibit the glide-reflection characteristics. Using aberration-corrected transmission electron microscope at the atomic scale, we have observed not only glide-reflection twins but also simple mirror-reflection twins in the $Al_{20}Cu_2Mn_3$ approximant. The two twinning modes are found to coexist in the present sample. These twins exhibit variant configurations at the twin boundaries where the tessellations of local subunits are imaged at an atomic scale. At the twin boundaries, diversified tiles such as star-like (*S*), bowtie-shaped and boat-shaped (*B*) are observed. The diversified tiles stacking with various manners allow the coexistence of the DQC and the approximant. Furthermore, the variants of *B* and *S* tiles are also found.

ARTICLE HISTORY
Received 8 October 2015
Accepted 18 June 2016

KEYWORDS
Transmission electron microscopy; decagonal approximant; twins; defects

1. Introduction

The $Al_{20}Cu_2Mn_3$ phase was reported by Raynor as early as in 1944 [1]. It is a B-centred orthorhombic structure with $a = 2.420$ nm, $b = 1.250$ nm, $c = 0.772$ nm, and the space group of *Bbmm* [2,3]. Recently, the atomic arrangements were proposed with the help of atomic-scale high-angle annular dark field-scanning transmission electron microscopy (HAADF-STEM) imaging, energy dispersive spectrum mapping and first-principles calculations [2,4]. Based on high-resolution transmission electron microscopy (HRTEM) observation, the subunits with hexagonal configuration in the $Al_{20}Cu_2Mn_3$ approximant were found to be tessellated in a parallel mode in (0 1 0) plane [5].

Twins are frequently observed in the $Al_{20}Cu_2Mn_3$ approximant, and two twinning models, namely, glide reflection twin and simple reflection twin, have been proposed [6–9]. Up to date, the glide reflection twins have been confirmed with the glide plane and glide vector being {1 0 1} and 1/4 [1 0 1], respectively. In contrast, the presence of twins with simple refection symmetry remains controversial [6].

CONTACT X. L. Ma xlma@imr.ac.cn
†Authors contributed equally in this work.

The crystalline approximants of a decagonal phase are full of various structural subunits, which may lead to many local tessellations with variant symmetries. Compared with the detailed studies on the defective structures in the T-Al-Mn-Pb and O-Al_3Co_4 phases which have similar structure to $Al_{20}Cu_2Mn_3$ [10–15], the information about the defective structures in $Al_{20}Cu_2Mn_3$ is still insufficient. Although glide reflection twin was directly imaged by HAADF-STEM technique [6], simple reflection twin was imaged by means of conventional coherent high-resolution TEM which is hard to directly extract atomic configurations at the twin boundary [7]. In this paper, we present the atomic structures of twins and various kinds of defective structures using HAADF-STEM technique under an aberration-corrected transmission electron microscope.

2. Experimental details

The 2024 aluminium alloy with the nominal composition of Al-4.35, Cu-1.55, Mg-0.53, Mn-0.11, Fe-0.13, Si-0.03, Ti (wt.%) is chosen for investigation. The $Al_{20}Cu_2Mn_3$ approximant of decagonal quasi crystal (DQC) is present in the as-received 2024 aluminium alloy. The alloy was first solid solution treated at 768 K followed by a water quench. Finally, the alloy was rolled to a tube at room temperature. The diameter of the rod-like $Al_{20}Cu_2Mn_3$ phase is about 30~200 nm. The sample was first cut into sections perpendicular to the deformation direction using a linear precision saw with the thickness of 600 μm and ground to about 100 μm thick by 1000 grit silicon carbide papers. The discs with diameter of 3 mm were prepared by die cutting, then mechanically ground, polished with diamond paste to 20 μm and finally thinned by ion milling.

Nanometer-scale structural investigations were performed in an aberration-corrected scanning transmission electron microscope operated at 300 kV (FEI Titan Cubed 60–300 kV microscope fitted with a high-brightness field emission gun (X-FEG), double Cs-correctors and a monochromator). In the STEM mode, the convergence angle of the electron beam is approximately 25 mrad, which yields a probe size less than 0.10 nm, and reaching a 0.07-nm resolution. Electron energy loss spectroscopy (EELS) spectra were collected with 0.5 eV per channel dispersion in the HAADF-STEM mode.

3. Results and discussion

3.1. Twinning models and structures in $Al_{20}Cu_2Mn_3$

The $Al_{20}Cu_2Mn_3$ approximant of the DQC with its *b* axis as the pseudo-ten-fold axis tends to form multiple twins easily, e.g. the glide reflection twin in Figure 1, which was confirmed in the previous study. Figure 1(a) is the HRTEM image of $Al_{20}Cu_2Mn_3$ taken along the *b* axis, showing a twin boundary (TB). Figure 1(b) and (c) is the [0 1 0] electron diffraction pattern (EDP) of the left domain and the composite [0 1 0] EDP of two domains, respectively. Two twinned reciprocal lattices in Figure 1(c) (as outlined) are mutually tilted by about 36°, in which one is the mirror reflection of the other with respect to the (1 0 1) plane. Figure 1(d) is the high-resolution HAADF-STEM image showing the twin boundary. The $Al_{20}Cu_2Mn_3$ is formed by a parallel tessellation of the flattened hexagons along the *b* axis, which are arranged in adjacent parallel rows and each unit cell contains two hexagonal (*H* for short) subunits. The elongated *H* subunits mutually tilted by about 36° at the TB. The twinning

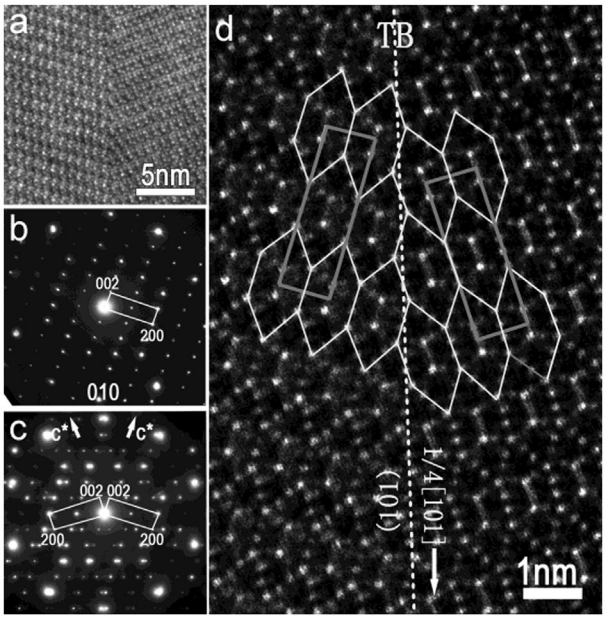

Figure 1. (a) HRTEM image of the $Al_{20}Cu_2Mn_3$ DQC approximant taken along the b axis, showing a twin boundary. (b) EDP of left domain with zone axis of [0 1 0]. (c) Composite EDP of the (1 0 1) twins with zone axis of [0 1 0]. Two twinned reciprocal lattices are outlined, one is the mirror reflection of the other with respect to the (1 0 1) plane mutually tilted by about 36°. (d) High-resolution HAADF-STEM image of the two domains.

exhibits glide reflection symmetry with the glide plane and glide vector being {1 0 1} and 1/4 [1 0 1], respectively. The glide reflection symmetry TB can stack easily by the *H* subunits. This kind of TB is the most common boundary in the $Al_{20}Cu_2Mn_3$ and was observed in the previous studies [5–7].

In the meanwhile, the previous studies [6–9] also indicate that a twining with reflection symmetry is theoretically possible. However, such a twinning mode has not been confirmed so far in experiments. Taking the geometry into account, the twin with reflection symmetry could not exist if *H*-subunit was the only structural block in the crystal. Otherwise, some special defects should appear at the TB to fill the gaps between the domains. In our observations, we frequently find the reflection symmetry twin with a novel TB, which is composed of a group of periodically bow-tie-shaped (BT for short) structure, as outlined in yellow in Figure 2(a). The two twinned domains are separated by periodic BT tiles which mutually tilt by about 36° without any gliding.

This novel TB is also found in some glide reflection symmetry twin. Figure 2(b) shows a twin having the same glide plane and glide vector as the twin in Figure 1, but the TB is composed of two rows of BT tiles. In the present observations, we find that the twin with the special BT subunit at the TB just occasionally occurs in the $Al_{20}Cu_2Mn_3$. Instead, the glide reflection twin stacked by the H subunits is frequently observed. This phenomenon could be interpreted in teams of the high formation energy of TB stacked by BT tiles.

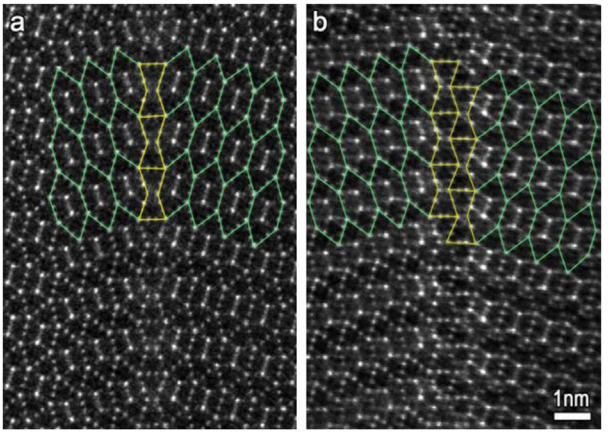

Figure 2. (colour online) (a) High-resolution HAADF-STEM image showing the reflection symmetry twining mode. The twin boundary is composed of periodic BT tiles. (b) High-resolution HAADF-STEM image showing a glide reflection symmetry twin. The twin boundary is composed of two rows of BT tiles.

3.2. Characteristics and configurations of the defective structure

The $Al_{20}Cu_2Mn_3$ particles in the present sample feature a rod-like morphology, with ⟨0 1 0⟩ as the longitudinal direction. The cross section image of a typical $Al_{20}Cu_2Mn_3$ particle taken along the b axis is shown in Figure 3(a). It is seen that the cross section is likely a polygonal apple. Figure 3(b) is the composite [0 1 0] EDP of the particle, showing a ten-fold symmetry. A HAADF-STEM image of the particle is shown in Figure 3(c), in which a curving line with a brighter contrast is seen. Since the image contrast in the HAADF imaging mode is strongly associated with the local variety of chemical composition and/or thickness contribution [16], the brighter contrast at the centre of the 'apple' implies that the local compositions are different from the neighbouring areas. We performed the EELS analysis in the HAADF-STEM mode to this specific area, which is shown in Figure 3(d)–(f). According to the distribution of Cu in Figure 3(d), it is seen that Cu is rich at the curving line with the brighter contrast. Furthermore, the outermost surface of the particle also shows a Cu-rich characteristic. Nevertheless, the apparent surface of the particle does not show a perceptible bright contrast in the HAADF-STEM image, which implies a possible depletion of another noble element like Mn.

Here, the structural characteristic of the centre enriched with Cu element is particularly focused. Based on the lattice parameters, the rotation angle of the twins in $Al_{20}Cu_2Mn_3$ is close not exactly to 36°. Therefore, the ten-fold twins cannot be of perfect ten-fold. Not all of the twin boundaries feature a regular rotation of 36°. Actually, in our present study, we find that the $Al_{20}Cu_2Mn_3$ particles are composed of less-than-ten twin domains. In addition, to the regular TB, irregular TBs composed of other structural units are also found. This is the case in the Cu-rich area as shown in Figure 3. The high-resolution HAADF-STEM image corresponding to the central area in Figure 3 is shown in Figure 4. It is seen that the nano-particle is composed of nine domains (numbered with I–IX) separated by TBs marked by yellow lines. The Cu element is enriched at the boundary between IX plate with the I, II and III plates (the rotation of these domains is about 72°, 108° and 144°), referring an irregular TB. Different from the regular TB, the irregular TB consists of a large number of complex

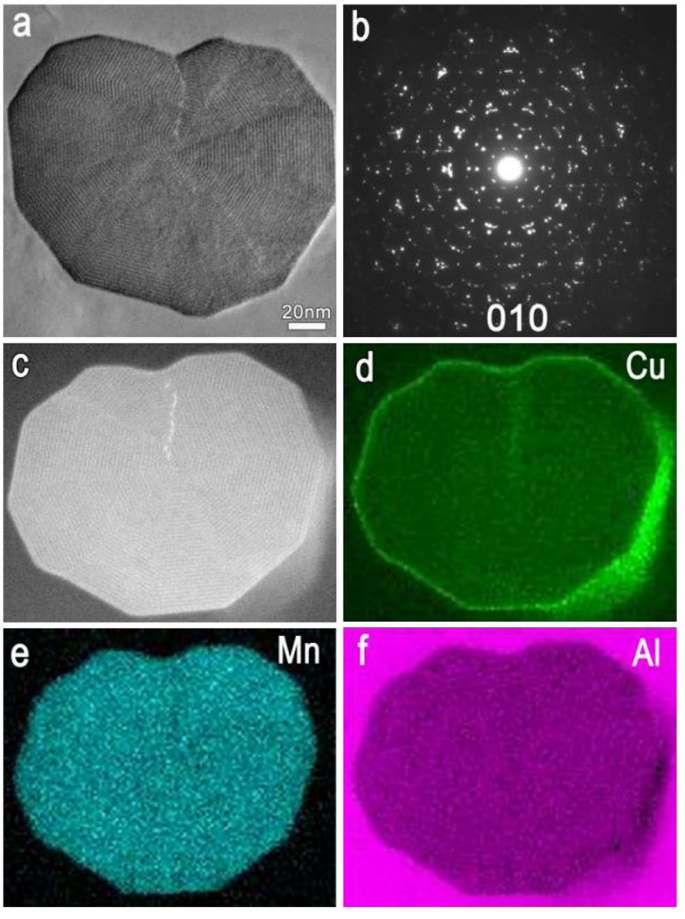

Figure 3. (colour online) (a) HRTEM image of a typical $Al_{20}Cu_2Mn_3$ apple-shaped particle taken along the b axis. (b) Composite EDP of the $Al_{20}Cu_2Mn_3$ particle with zone axis of [0 1 0]. (c) An HAADF image of an $Al_{20}Cu_2Mn_3$ particle along the crystallographic [0 1 0] direction. Note the brighter contrast at the centre of the particle, which implies a segregation of the heavier elements. (d)–(f) EELS mapping analysis showing the heterogeneous distribution of the compositional elements of Cu, Mn, Al.

linear defects, which take on diversified polygonal shapes from the various arrangements of the surrounding H subunits. Two of the complex defects are outlined and shown in Figure 4(c) and (d). It is seen that the shape of the defects is random and the atomic arrangement in these complex defects seems disorder. It was noted that the pronounced redistribution of the component atoms tends to occur around defects as a result of the total free energy reduced due to solute atoms segregated at the defect [17]. Correspondingly, the Cu enrichment in the present study occurs at the irregular boundary.

At the boundary of domain II and III, we find rows of elongated hexagons in alternating orientation, which represent a fault in the stacking sequence of the hexagonal rows. This type of planar defect can be referred to a stacking fault or a micro twin. The alternation of two differently oriented hexagon-slabs corresponds to the Y-AlMnCu [5], which is another approximant of the AlMnCu DQC. The unit cell of Y-AlMnCu is labelled with a red rectangle in Figure 4(b) and it is seen that each unit cell contains two *H* tiles.

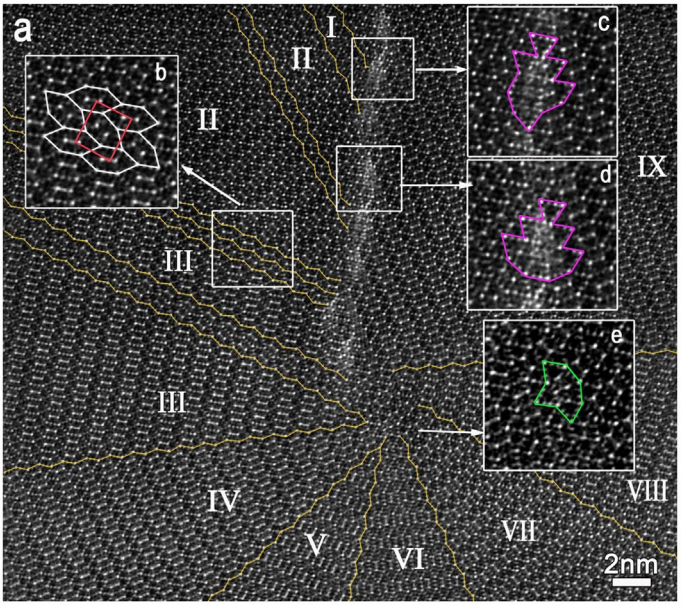

Figure 4. (colour online) (a) High-resolution HAADF-STEM image showing the zoom-in image of the central area in the particle shown in Figure 3. It is seen that the particle is composed of nine twin domains (marked with I–IX). (b) Elongated hexagons in alternating orientation. (c) and (d) Two complex defective structures are outlined. It is seen that the configurations of these defective structures are random and the atomic arrangements therein seem disordered. (e) A boat-shaped tile in the domain junction zone is outlined in which the atomic arrangement is ordered.

Compared with the complex defects in the irregular TB, diversified tiles with fixed shapes are frequently observed in the junction zone of twin domains. As shown in Figure 4(e), a boat-shaped tile (*B* tile for short) is outlined, where the atomic arrangement is ordered. Such a type of tiles can be outlined as various regular shapes. Figure 5 shows a high-resolution HAADF-STEM image at the conjunction area of several twin domains. It is worthwhile to mention that each TB terminates at a *B* tile and diversified tiles exist in the interface of twin domains. Usually, these diversified tiles can be outlined as three fixed shapes, e.g. boat, bow-tie and star, as shown in Figure 5. These tiles are formed by differently oriented H subunits stacking with various modes and always form at the centre of the twinning domains. These kinds of tiles were found in other quasicrystals and their crystalline approximants [18–20].

According to the previous work, the *H*, *B* and star-shaped tiles (*S* tiles for short) can be derived from the structure of many kinds of DQCs [21,22]. This indicates that both the defect tiles (*B* and *S* tiles) and the subunit tiles (*H* tiles) are the basic structure tiles in a DQC. Figure 6(a) shows a HAADF-STEM image of an $Al_{20}Cu_2Mn_3$ particle with a bright contrast in the black rectangular. It can be found that this is the centre of twin domains and it contains high density of regular defect tiles. A nano-sized core structure of DQC is outlined based on *H*, *B* and *S* tiles.

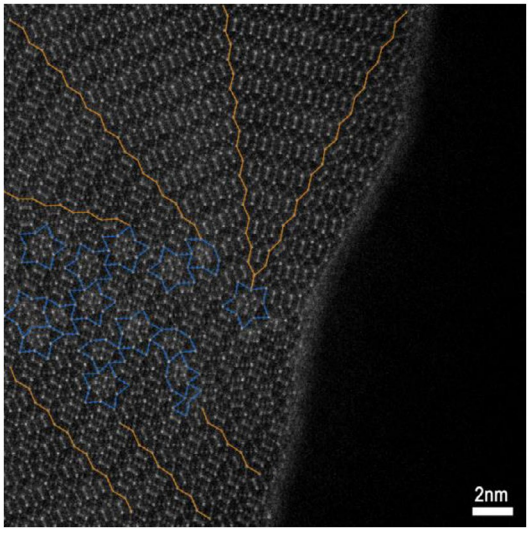

Figure 5. (colour online) High-resolution HAADF-STEM image of the conjunction zone area of several twin domains showing an intergrowth of *B*, *S* and BT tiles.

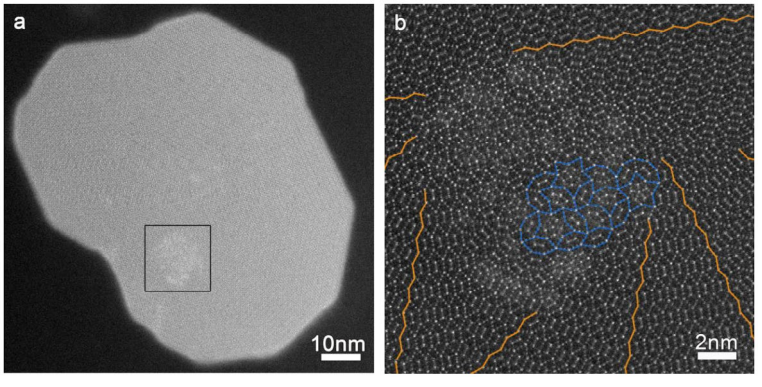

Figure 6. (colour online) (a) HAADF-STEM image of an $Al_{20}Cu_2Mn_3$ particle with a brighter contrast core which was marked with the black rectangular. (b) Zoom-in image of the area in the black rectangular. The core contains a nano-sized decagonal quasicrystal.

3.3. Structural variants of B and S tiles

Taking atomic positions into account, both *B* and *S* tiles exhibit structural variants. According to the atomic arrangement in $Al_{20}Cu_2Mn_3$ [6], the dark and light blue dots in Figure 7 represent the Mn atom columns with different densities along the [0 1 0] line direction, and the green dots represent the Cu atom columns. The locations of Al atom columns are ignored due to the dark contrast in the HAADF mode. Figure 7(a) is a high-resolution HAADF-STEM image of a twin with reflection symmetry, where the boundary is not only stacked by a row of BT tiles, but also accompanied by *B* tiles. Figure 7(b) and (c) shows the enlarged images of two B tiles and their differences are schematically shown in Figure 7(d) and (e). It is seen that the B tile in Figure 7(b) is composed of a BT tile and an *H* tile. However, the

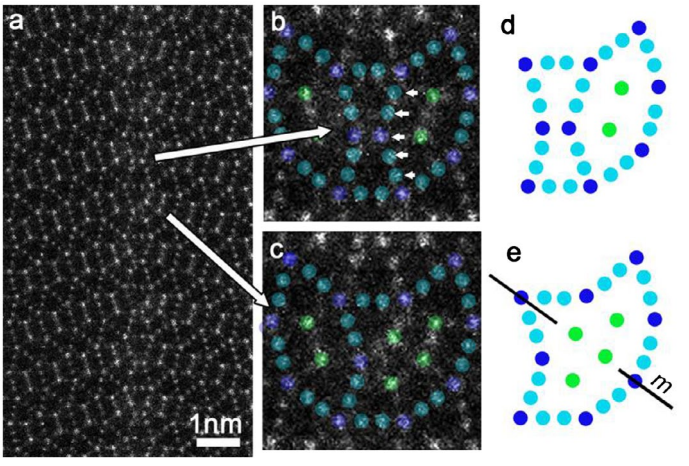

Figure 7. (colour online) (a) High-resolution HAADF-STEM image shows a reflection symmetry twin with the twin boundary composed of BT tiles. (b) High-resolution image of a BT tile in the middle of two hexagon tiles with reflection symmetry is revealed by the sub-transparent dots. (c) The arrangement of the atoms arrowed by white in Figure 7b has changed and a boat-shaped tile with reflection symmetry is present. (d)–(e) Schematic model of the tiles in (b)–(c) denoted by dots.

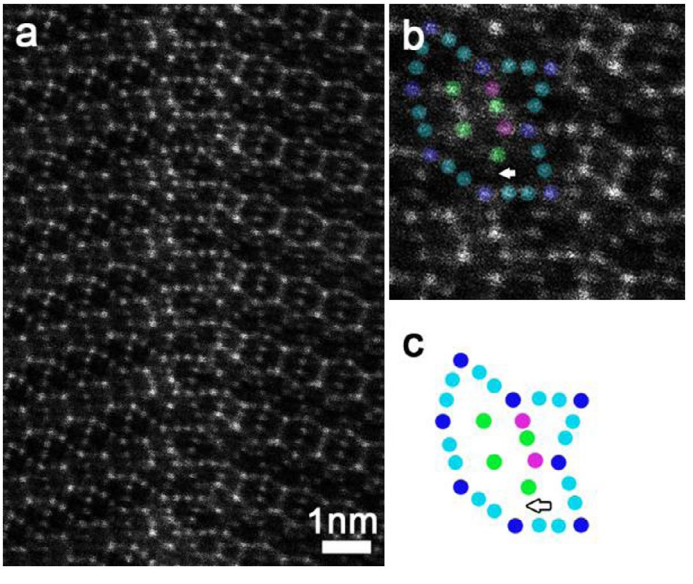

Figure 8. (colour online) (a) High-resolution HAADF-STEM image showing a glide reflection twin structure. (b) Zoom-in image of the twin boundary showing a variant of *B* tile in which the atomic arrangement is different from *B* tile. (c) Schematic model of the variant in (b) denoted by dots.

B tile in Figure 7(c) has a mirror by rearrangement of several atoms position arrowed by white arrows in Figure 7(b), breaking the combination of BT and *H* in Figure 7(b). The third variant of *B* tile is shown in Figure 8, where some atom are slightly rearranged from that of Figure 7(b).

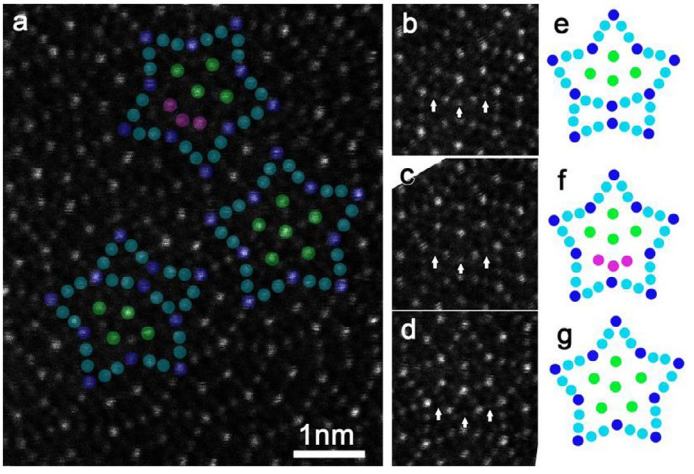

Figure 9. (colour online) (a) High-resolution HAADF-STEM image showing three S tiles outlined with dots. The atomic arrangements are different in the interior of the three *S* tiles. (b) The *S* tile is in fact composed of a BT and a *B* tile. (c) The contrast of two atom columns arrowed in white becomes shallow and even disappears. (d) The contrast of two atom columns arrowed in white disappears and thus the *S* tile shows a five-fold symmetry. (e)–(f) The schematic illustration corresponding to (b)–(d).

In addition to the structural variants of *B* tiles, we also found variants for *S* tiles, as seen in the high-resolution HADDF-STEM image in Figure 9(a). The individual images of three types of *S* tiles and the corresponding schematic diagrams are given in Figure 9(b)–(g), respectively. We notice that the atomic arrangements in the interior of the three *S* tiles are different. The *S* tile in Figure 9(g) has a five-fold rotation symmetry, while the others in Figure 9(e) and (f) are broken in five-fold symmetry. We found that the three *S* variants in Figure 9 can be geometrically transferred with each other, through adjusting the positions of the atom columns indicated by white arrows in Figure 9(b)–(d). Consequently, the variants in Figure 9(e) and (f) can be regarded as the combination of *S* and BT tile, while the *S* in Figure 9(g) has a perfect five-fold symmetry. Note that two atomic columns are missed in the BT tile in Figure 9(f), compared with that in Figure 9(e).

We would like to add that in the 1980–1990s, when the quasicrystals and their crystalline approximants were extensively investigated, the crystallographic information was basically limited to the level of lattice, little information was on atomic configurations in the unit cell or at the defective areas; particularly at that time, coherent high-resolution TEM imaging mode was widely used which cannot provide direct *Z*-contrast images to show atomic configurations. The new information in our present work is to show not only the refection twin in $Al_{20}Cu_2Mn_3$ decagonal approximant but also atomic configurations at the boundary of the simple reflection twin.

4. Conclusion

We have identified the two models of twin reflection symmetry at an atomic level in the $Al_{20}Cu_2Mn_3$ approximant by aberration-corrected transmission electron microscope. Two novel structures of TB with the stacked bowtie-shaped tiles are observed. Moreover, we

found some twins which are rich of Cu along the TB. Comparatively, regular defects with fixed shapes, like bowtie-shaped tile, *B* tile and *S* tile, are usually formed at the interface of the twin domains. By the stacking of *H*, *B* and *S* tiles, the DQC and the approximant coexist in the $Al_{20}Cu_2Mn_3$ particles. Finally, we found several variants of the *B* and *S* tile, whose structures can be transferred with each other geometrically through the adjustment of several atomic positions.

Disclosure statement

No potential conflict of interest was reported by the authors.

Funding

B. Zhang acknowledges the National Natural Science Foundation of China [grant number 51101157] and the Innovation Fund in IMR [grant number SCJJ-2013-PY-09]. Z. B. He acknowledges the Self-determined Project of State Key Laboratory for Advanced Metals and Materials, University of Science and Technology Beijing [grant number 2014Z-03], the National Natural Science Foundation of China [grant number 51471024] and the Fundamental Research Funds for the Central Universities, China.

References

[1] G. Raynor, *The constitution of the aluminium-rich aluminium-manganese-nikel alloys,* J. Inst. Metals 70 (1944), pp. 507–529.
[2] K. Robinson, *The determination of the crystal structure of Ni4Mn11Al60,* Acta Crystallogr. 7 (1954), pp. 494–497.
[3] S.C. Wang, C.Z. Li, and M.G. Yan, *Determination of structure of al20cu2mn3 phase in al-cu-mn alloys*, Mater. Res. Bull. 24 (1989), pp. 1267–1270.
[4] A. Damjanovic, *Structure analysis of T3(AlMnZn) compound*, Acta. Crystallogr. 14 (1961), pp. 982–987.
[5] X.Z. Li and K.H. Kuo, *Orthorhombic crystalline approximants of the Al-Mn-Cu decagonal quasi-crystal*, Philos. Mag. Part B 66 (1992), pp. 117–124.
[6] Z. Shen, C. Liu, Q. Ding, S. Wang, X. Wei, L. Chen, J. Li, and Z. Zhang, *The structure determination of $Al_{20}Cu_2Mn_3$ by near atomic resolution chemical mapping*, J. Alloys Compd. 601 (2014), pp. 25–30.
[7] Y. Chen, D. Yi, Y. Jiang, B. Wang, D. Xu, and S. Li, *Twinning and orientation relationships of T-phase precipitates in an Al matrix*, J. Mater. Sci. 48 (2013), pp. 3225–3231.
[8] Z.Q. Feng, Y.Q. Yang, B. Huang, M.H. Li, Y.X. Chen, and J.G. Ru, *Crystal substructures of the rotation-twinned T ($Al_{20}Cu_2Mn_3$) phase in 2024 aluminum alloy*, J. Alloys Compd. 583 (2014), pp. 445–451.
[9] Z. Chen, P. Chen, and S. Li, *Effect of Ce addition on microstructure of $Al_{20}Cu_2Mn_3$ twin phase in an Al–Cu–Mn casting alloy*, Mater. Sci. Eng. A 532 (2012), pp. 606–609.
[10] H. Klein and M. Feuerbacher, *Structure of dislocations and stacking faults in the complex intermetallic xi '-(Al-Pd-Mn) phase*, Philos. Mag. 83 (2003) pp. 4103–4122.
[11] M. Heggen, L. Houben, and M. Feuerbacher, *Plastic-deformation mechanism in complex solids*, Nat. Mater. 9 (2010), pp. 332–336.
[12] M. Heggen, L. Houben, and M. Feuerbacher, *Metadislocations in the structurally complex orthorhombic alloy Al13Co4*, Philos. Mag. 88 (2008), pp. 2333–2338.
[13] M. Heidelmann, M. Heggen, C. Dwyer, and M. Feuerbacher, *Comprehensive model of metadislocation movement in Al13Co4*, Scr. Mater. 98 (2015), pp. 24–27.
[14] M. Heggen and M. Feuerbacher, *Core structure and motion of metadislocations in the orthorhombic structurally complex alloy $Al_{13}Co_4$*, Mater. Res. Lett. 2 (2014), pp. 146–151.

[15] I. Černičková, P. Švec, S. Watanabe, Ľ. Čaplovič, M. Mihalkovič, V. Kolesár, P. Priputen, J. Bednarčík, D. Janičkovič, and J. Janovec, *Fine structure of phases of epsilon-family in Al73.8Pd11.9Co14.3 alloy*, J Alloy Compd. 609 (2014), pp. 73–79.
[16] S.J. Pennycook, *Structure determination through Z-contrast microscopy*, Adv. Imag. Elect. Phys. 123 (2002), pp. 173–206.
[17] R. Kirchheim, *Reducing grain boundary, dislocation line and vacancy formation energies by solute segregation. I. Theoretical background*, Acta Mater. 55 (2007), pp. 5129–5138.
[18] L. Beraha, M. Duneau, H. Klein, and M. Audier, *Correlated phason jumps involved in plastic deformation of Al-Pd-Mn approximant phases*, Philos. Mag. A 76 (1997), pp. 587–613.
[19] H. Klein, M. Boudard, M. Audier, M. De Boissieu, H. Vincent, L. Beraha, and M. Duneau, *The T-Al-3(Mn, Pd) quasicrystalline approximant: Chemical order and phason defects*, Philos. Mag. Lett. 75 (1997), pp. 197–208.
[20] H. Klein, M. Feuerbacher, P. Schall, and K. Urban, *Novel type of dislocation in an Al-Pd-Mn quasicrystal approximant*, Phys. Rev. Lett. 82 (1999), pp. 3468–3471.
[21] X.Z. Li, J.M. Dusois, and K.H. Kuo, *2-color penrose tiling*, Philos. Mag. Lett. 69 (1994), pp. 93–98.
[22] P. Gummelt, *Random cluster covering model*, J. Non-Cryst. Solids 334–335 (2004), pp. 62–67.